doi:10.20944/preprints201811.0536.v1

Article

Facile Fabrication of Multifunctional ZnO Urchins on Surfaces

Abinash Tripathy[‡,¥], Patryk Wąsik[‡,ψ], Syama Sreedharan[‖], Dipankar Nandi[‖], Oier Bikondoa[†,£], Bo Su[§], Prosenjit Sen[¥] and Wuge H. Briscoe[‡]*

[‡] - School of Chemistry, University of Bristol, Cantock's Close, Bristol BS8 1TS, United Kingdom.

[¥] - Centre for Nano Science and Engineering, Indian Institute of Science, Bangalore, India, 560012.

[ψ] - Bristol Centre for Functional Nanomaterials (BCFN), HH Wills Physics Laboratory, University of Bristol, Tyndall Avenue, Bristol BS8 1TL, United Kingdom.

[‖] - Department of Biochemistry, Indian Institute of Science, Bangalore, India, 560012.

[†] - XMas, The UK CRG Beamline at the ESRF, The European Synchrotron, 71, avenue des Martyrs, CS 40220, 38043 Grenoble Cedex 9, France.

[£] - Department of Physics, University of Warwick, Gibbet Hill Road, CV4 7AL, Coventry, United Kingdom.

[§] - Bristol Dental School, University of Bristol, Bristol BS1 2LY, United Kingdom.

*Corresponding Author: Wuge.Briscoe@bristol.ac.uk

Abstract: Functional ZnO nanostructured surfaces are important in a wide range of applications. Here we report facile fabrication of ZnO surface structures at near room temperature with morphology resembling that of sea urchins, with densely packed, μm-long, tapered nanoneedles radiating from the urchin centre. The ZnO urchin structures were successfully formed on several different substrates with high surface density and coverage, including silicon (Si), glass, polydimethylsiloxane (PDMS), and copper (Cu) sheets, as well as Si seeded with ZnO nanocrystals. Time-resolved SEM revealed growth kinetics of the ZnO nanostructures on Si, capturing the emergence of "infant" urchins at the early growth stage and subsequent progressive increase in the urchin nanoneedle length and density, whilst the spiky nanoneedle morphology was retained throughout the growth. ε-Zn(OH)$_2$ orthorhombic crystals were also observed alongside the urchins. The crystal structures of the nanostructures at different growth time were confirmed by synchrotron X-ray diffraction measurements. On seeded Si substrates, a two-stage growth mechanism was identified, with a primary growth step of vertically aligned ZnO nanoneedle arrays preceding the secondary growth of the urchins atop the nanoneedle array. The antibacterial, anti-reflective, and wetting functionality of the ZnO urchins – with spiky nanoneedles and at high surface density – on Si substrates was demonstrated. First, bacteria colonisation was found to be suppressed on the surface after 24 h incubation in Gram-negative *E. coli* culture, in contrast to control substrates (bare Si and Si sputtered with 20 nm ZnO thin film). Secondly, the ZnO urchin surface, exhibiting superhydrophilic property with a water contact angle $\sim 0°$, could be rendered superhydrophobic with a simple silanization step, characterised by a water static contact angle θ of 159°±1.4° and contact angle hysteresis $\Delta\theta < 7°$. The dynamic superhydrophobicity of the surface was demonstrated by bouncing-off of a falling 10 μL water droplet, with a contact time of 15.3 milliseconds (ms), captured using a high-speed camera. Thirdly, it was shown that the presence of dense spiky ZnO nanoneedles and urchins on the seeded Si substrate exhibited a reflectance R < 1% over the wavelength range $\lambda = 200\text{-}800$ nm. The ZnO urchins with unique morphology *via* a facile fabrication route at room temperature, readily implementable on different substrates, may be further exploited for multifunctional surfaces and product formulations.

Keywords: ZnO urchins, nanostructured surfaces, E. coli, superhydrophilic, superhydrophobic, anti-reflective surfaces

---

1. Introduction

Nanostructured surfaces are widespread in nature and many are ingeniously multifunctional. This has inspired considerable effort in fabrication of hierarchical surface nanotextures. For instance, Lotus leaf inspired nanostructures on silicon, TiO_2, polymer surfaces exhibit superhydrophobic, self-cleaning and antibacterial characteristics[1–5]. Nanostructured surfaces on silicon, glass substrates mimicking cicada/dragonfly wings or moth eye possess superhydrophobic and antimicrobial characteristics, as well as gradient refractive indices for anti-reflective applications[6–11].

Surfaces bearing ZnO nanostructures are among most widely studied, with a wide range of applications in gas and bio-sensing, field emission devices, ultra violet detectors, and photovoltaics[12], due to their thermostability[13], low-cost production[14], antimicrobial properties[15–19], and biocompatibility[20]. Several fabrication methods of ZnO nanostructured surfaces have been reported[21–28], such as hydrothermal synthesis, laser ablation, sputtering, thermal decomposition, evaporation induced self-assembly[29,30], and the sol-gel technique. Various ZnO nanostructures that have been reported include one-dimensional (1-D) morphologies such as nanowires[31–33], nanorods[34–37], and nanotubular structures[38–42], as well as 3-D architectures such as flowers/urchins[43–48], tetrapods/jack-like[49,50], and hedgehogs[51]. The 3-D nanostructures with enhanced surface area may be used as substitutes for 1-D nanostructure arrays with enhanced functionalities, but their fabrication requires either sophisticated instrumentation or elevated temperatures (thus high energy input).

Here, we report facile fabrication of multifunctional 3-D ZnO urchins on silicon (Si) substrates in a solution-based synthesis at near room temperature (RT) using a one-step procedure, which could also be applied on Si substrates seeded with ZnO crystals and various other substrates. The morphology of these ZnO surface structures resembles that of sea urchins, with tapered nanoneedles of m in length radiating from a central core. The growth kinetics of the ZnO urchins was studied by examining their intermediate morphologies at different growth time intervals (0.5 - 12 h). The ZnO urchin-coated surface exhibited high anti-reflectance, and superhydrophobicity after silanization as investigated by contact angle, contact angle hysteresis and drop impact analyses. They were also bacteriophobic against *E. coli*. The simple fabrication method for ZnO urchins could also be adapted to a variety of materials such as polydimethylsiloxane (PDMS), copper sheets and glass substrates, demonstrating its versatility.

2. Materials and Methods

2.1 Substrates preparation and cleaning

Silicon substrates were prepared by cutting a silicon wafer (100 mm diameter, P type, B dopant, <100>, 1-100 Ω·cm, 500 μm thick, single-sided polish, test grade, University Wafer, Inc.) into 1 cm x 1 cm squares. All substrates, including copper sheet, glass slide (Polar Industrial Corporation) and polydimethylsiloxane (Dow Corning, Sylgard 184) were cleaned by a subsequent sonication in acetone, ethanol, and deionized water (10 minutes in each) followed by drying with N_2.

2.2 Seeding

Seeding procedure was used to produce nucleation sites for the growth of ZnO nanostructures[31]. Cleaned silicon substrates were dipped in a solution of zinc acetate dihydrate ($Zn(CH_3COO)_2{\cdot}2H_2O$, 99%, Sigma Aldrich) in ethanol (CH_3CH_2OH, Absolute, Sigma Aldrich) for few seconds, rinsed with clean ethanol and then dried with N_2. This coating step was repeated 5 times for each seeded silicon substrate (see Figure S1). Subsequently, the substrates were heated to 300° C on a hot plate, and annealed for 30 minutes in air to thermally decompose zinc acetate crystallites to ZnO islands with (0001) planes parallel to the silicon substrate surface[31].

2.3 ZnO Urchin growth

To grow the ZnO nanostructures, 50 mL aqueous solution of zinc nitrate hexahydrate ($Zn(NO_3)_2{\cdot}6H_2O$, 98%, Sigma Aldrich) solution was added dropwise to 50 mL of potassium hydroxide (KOH, 85%, Fisher Scientific) aqueous solution under constant stirring for 30 minutes. Next, the alkali solution of zincate ions was carefully poured to the glass Petri dish containing substrates (seeded Si, non-seeded Si, Cu sheet, glass and polydimethylsiloxane, separately for each type) sealed with a glass lid and a paraffin film, and kept at $20° \pm 2°C$ for 12 hours. After the synthesis, samples were rinsed with DI water and dried with N_2.

2.4 Bacterial growth conditions and sample preparation

Isolated single colonies of *E. coli* K-12 (MG 1655) were used to prepare the pre-inoculum[52]. The culture was grown in Luria Bertani (LB) medium for 8 hrs at 37°C with constant shaking at 160 rpm. A 0.2 % pre-inoculum was added into 10 mL of LB medium and it was allowed to grow until 0.3 optical density (O. D.) at 600 nm[53]. The cells were subsequently pelleted and washed with phosphate-buffered saline (PBS). A cell suspension of 0.01 O. D. at 600 nm was used for studying the bacterial interaction with the bare, unmodified silicon, silicon with 20 nm thin film of ZnO and ZnO nano-urchin surfaces.

2.5 Scanning electron microscopy (SEM)

ZnO nanostructured surfaces were imaged using field emission scanning electron microscopy (JSM-IT300 SEM (JEOL)). Dimension of the ZnO nano urchin-like structures were obtained from the SEM images using ImageJ software. For bacterial sample imaging, substrates were first washed with PBS to remove the loosely adhered cells. Substrates were then dipped in 2.5% of Glutaraldehyde to fix the cells. After that all the substrates were allowed to dry in vacuum. Thin layer of gold (15 nm) was sputtered on the samples using a Quorum sputter coater (Q150T) to avoid the charging effect while doing the SEM. Samples were scanned thoroughly using SEM (sample size 1.3 cm × 1.3 cm) and the imaging was done in triplicates for all the samples. Selecting three specimens from each type of a sample (two controls and one ZnO Urchin surface) ensured the repeatability.

2.6 Urchin dimension analysis

ImageJ[54] was used to obtain the morphological information of the nanoneedles comprising the ZnO urchin and the vertical nanoneedles using the length and angle measurement tools.

2.7 X-ray Diffraction (XRD)

The presence of crystalline ZnO after the growth procedure was confirmed using D8 Advance Bruker-AXS diffractometer (Cu Kα radiation (λ = 0.154178 nm), $\theta - 2\theta$ scan, 2θ = 10°-90°, step size - 0.02 (2θ), step count - 1.5 s).

2.8 Grazing incidence X-ray diffraction (GIXRD)

GIXRD analysis of the seeded and non-seeded silicon substrates used to study the time dependence growth of ZnO nanostructures was performed at Beamline BM28 at the European Synchrotron Radiation Facility (France). Experimental parameters: radiation wavelength: 0.8856 Å, sample to detector distance: 0.24 m, detector: MAR165, calibrant: Silver behenate and ZnO powder. The diffraction patterns were reduced to one-dimensional line profiles using *pyFAI*, a pythonic library for 1D azimuthal / 2D radial integrations of diffraction images[55].

2.9 Contact angle measurement and high-speed imaging

Static contact angle measurements were carried out using a Krüss Drop Shape Analyser (DSA 100). 10 μL water droplet was placed gently on all the substrates to measure the contact angles. A droplet impact dynamics of water droplet on the superhydrophobic surface (salinized seeded silicon substrate with ZnO nanostructures) was captured using a high-speed camera (Photron FastCam SA4) at 10,000 fps (time resolution of 0.1 ms). The droplets were created by a micro-pipette and released from a height of 7 cm (Weber number $(We) = \frac{inertial\ force}{surface\ tension\ force} = \frac{\rho V^2 D_w}{\gamma} = \frac{1000 \times 1.17^2 \times 0.0026}{0.072} = 49$, $Density\ of\ water\ (\rho) = 1000\frac{kg}{m^3}, Velocity\ of\ falling\ droplet\ (V) = \sqrt{2gh} = 1.17\frac{m}{s}, Surface\ tension\ of\ water\ (\gamma) = 0.072\frac{N}{m}$, and $diameter\ of\ droplet\ (D_w) = 0.0026\ m$).

2.10 Reflectance measurements

To calculate the reflectance of all the surfaces, Shimadzu MPC3600 UV-VIS-NIR Spectrometer with an absolute specular reflectance mode was used. Wavelengths ranging from 200 nm to 800 nm were used for the reflectance measurement. D_2 light source was used for the range 200 nm – 310 nm and Tungsten source was used for the range 310 nm – 800 nm. The angle of incidence and angle of reflection were set to 5° throughout the experiment. The equipment used a photomultiplier tube (PMT) detector. The reflectance from a surface is evaluated by its refractive index profile[6]. In general, a flat surface has a high reflectance due to the discontinuous refractive index profile, whereas structured surface suppresses reflection with its graded refractive index profile[6].

3. Results and Discussion

Figure 1 shows the SEM images of densely packed urchins after growth in 5 mM zincate solution on a seeded silicon substrate (Figure S2) at ~20° C for 12 h, and the simple fabrication method is described in Figure S1. XRD (Figure S11) confirmed that these urchins were ZnO. The morphology of an individual urchin (Figure 1c) reveals sharply tapered needles radiating from the centre. The length of the needles was $L \sim 1.65 \pm 0.11$ µm, its width at the central base $D_c \sim 156 \pm 24$ nm and at the tip $D_t \sim 13 \pm 7$ nm, with a tapering angle $\theta \sim 10^o$ and an average tip-to-tip spacing $s \sim 504 \pm 119$ nm (see Figure S3- S5 for the size distribution analysis).

Previously, ZnO nano- and micro-structures bearing resemblance of the urchin morphology have been reported. For instance, Elias et al.[48] prepared µm-sized hollow spheres with a ZnO nano-columns coating using atom layer deposition and electrodeposition, whilst the method by Shen et al.[47] used thermos-evaporation of metallic Zn powder at high temperature (~750^{o}C). Wahab et al.[43] fabricated ZnO nano-flowers blunt tapering via pH-controlled reactions in solution of zinc acetate dihydrate and sodium hydroxide at 90^{o}C. Using a similar approach, Gokarna et al.[44] synthesised ZnO urchin-like structures with columnar nanoneedles. Hieu et al.[45] sputtered zinc onto a polystyrene-sphere array and subsequent oxidation at 500^{o}C led to columnar ZnO urchins ; and the method by Taheri et al.[46] also involved depositing zinc acetate dihydrate precursor followed by calcination at 500^o C. The solution synthesis method we report here is relatively much simpler (at RT and applicable to different surfaces as we show below) compared to these previous studies, producing spiky tapered morphology of the urchin needles with a very high density previously unreported. The presence of high density spiky ZnO urchins endows the surface with multi-functionalities as discussed below.

SEM images of the region not covered by the urchins reveal vertical ZnO nanoneedles (from the primary growth step as referred to in Figure 1d, g) with an average base diameter ~ 90±20 nm, smaller than that of the urchin needles (Figure 1d-g), and the cross-section SEM view confirms that the ZnO urchins were formed atop a layer of nanoneedle arrays (Figure 1a, b). Orthorhombic ε-$Zn(OH)_2$ crystals with facet edges ~10-30 µm were also observed (Figure S7), with ZnO urchins (the secondary growth in Figure 1d) decorating the facets. The tapered or spiky nanoneedle geometry might be attributed to the concentration gradient of the zinc ions in the vicinity of the substrate where the ZnO nanocrystal seeds provided the nucleation sites for ZnO nanoneedles growth (Figure 1f, g)[56].

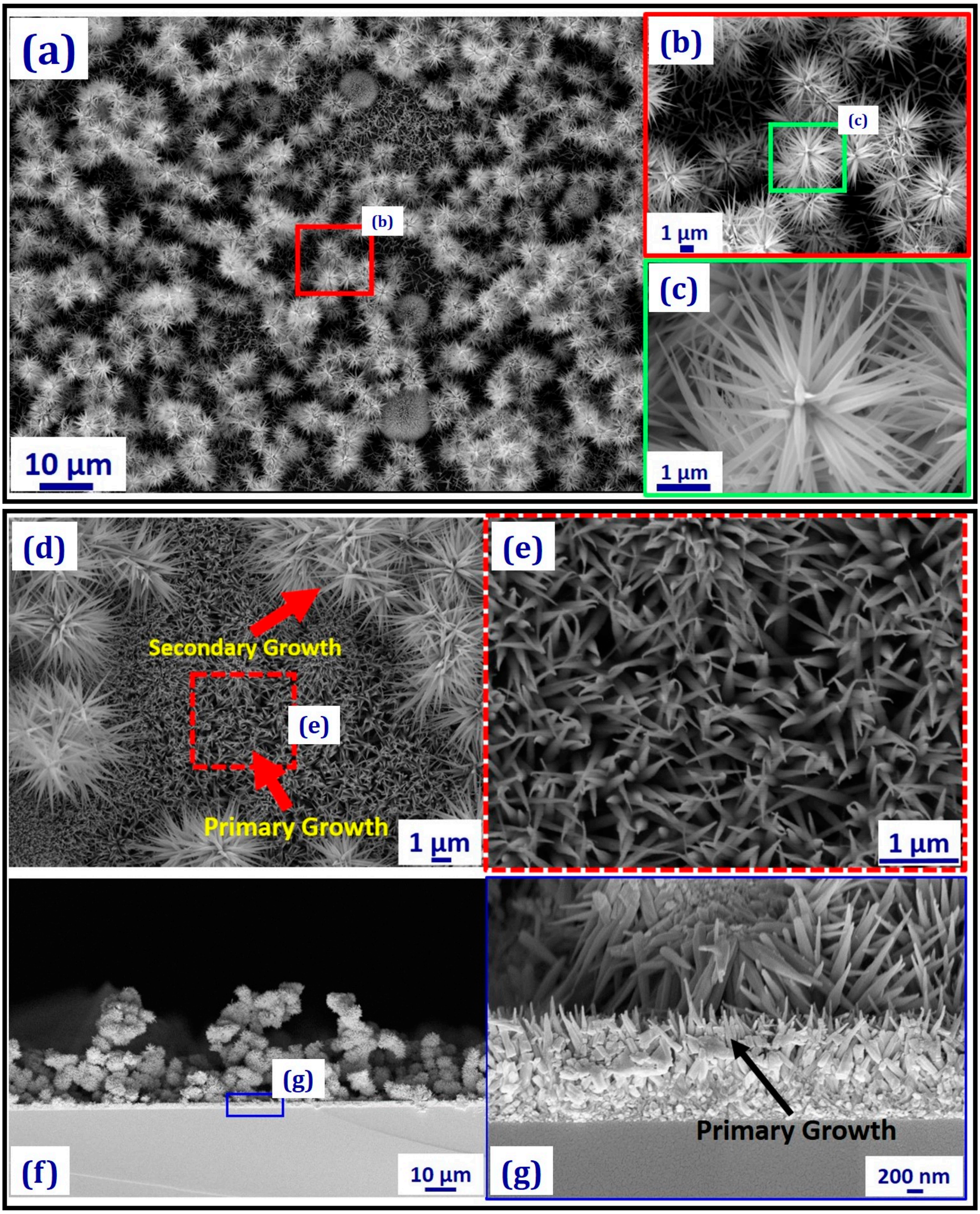

Figure 1: (a) Scanning electron microscopy (SEM) images of ZnO urchins on a seeded silicon substrate; (b) SEM images depicting the ZnO urchin and primary vertical nanoneedle growth on the silicon substrate. SEM images show random multidirectional growth of the nanoneedles comprising the urchin (seeding concentration of zinc acetate dihydrate - 5 mM, synthesis time for ZnO urchin growth - 12 h, and temperature - 20° C).

To understand the growth kinetics of the ZnO nanostructures, SEM images (Figure 2, Figure S8 and S9) of the seeded silicon substrates were taken at different growth time intervals *t*. At *t* = 0.5-1 h (Figure 2a, b), only the primary growth of vertical nanoneedle structures was observed. At *t* = 3 h, the secondary growth of urchin-like structures atop the nanoneedle array with a diameter ϕ ~1μm was observed. The density and size of the urchins and length of the urchin needle *L* then increased with time (see Figure S5 for urchin needle length *L vs.* growth time *t*), whilst the tapering angle remained largely constant at θ ~10°. Figure 2g presents the GIXRD data (see section II.4. in supplementary information) on the seeded silicon substrates at different growth time intervals. The intense (002) ZnO peak at $t < 3$h is consistent with the primary growth of vertical ZnO nanoneedles. The ε-Zn(OH)$_2$ phase (orthorhombic crystals) is visible for the samples with reaction time $t > 3$ h (**Error! Reference source not found.**). This shows that the ZnO nanoneedles started forming after 30 min and Zn(OH)$_2$ crystals after 3 h, likely together with the secondary growth of ZnO urchins (Figure 2c-f).

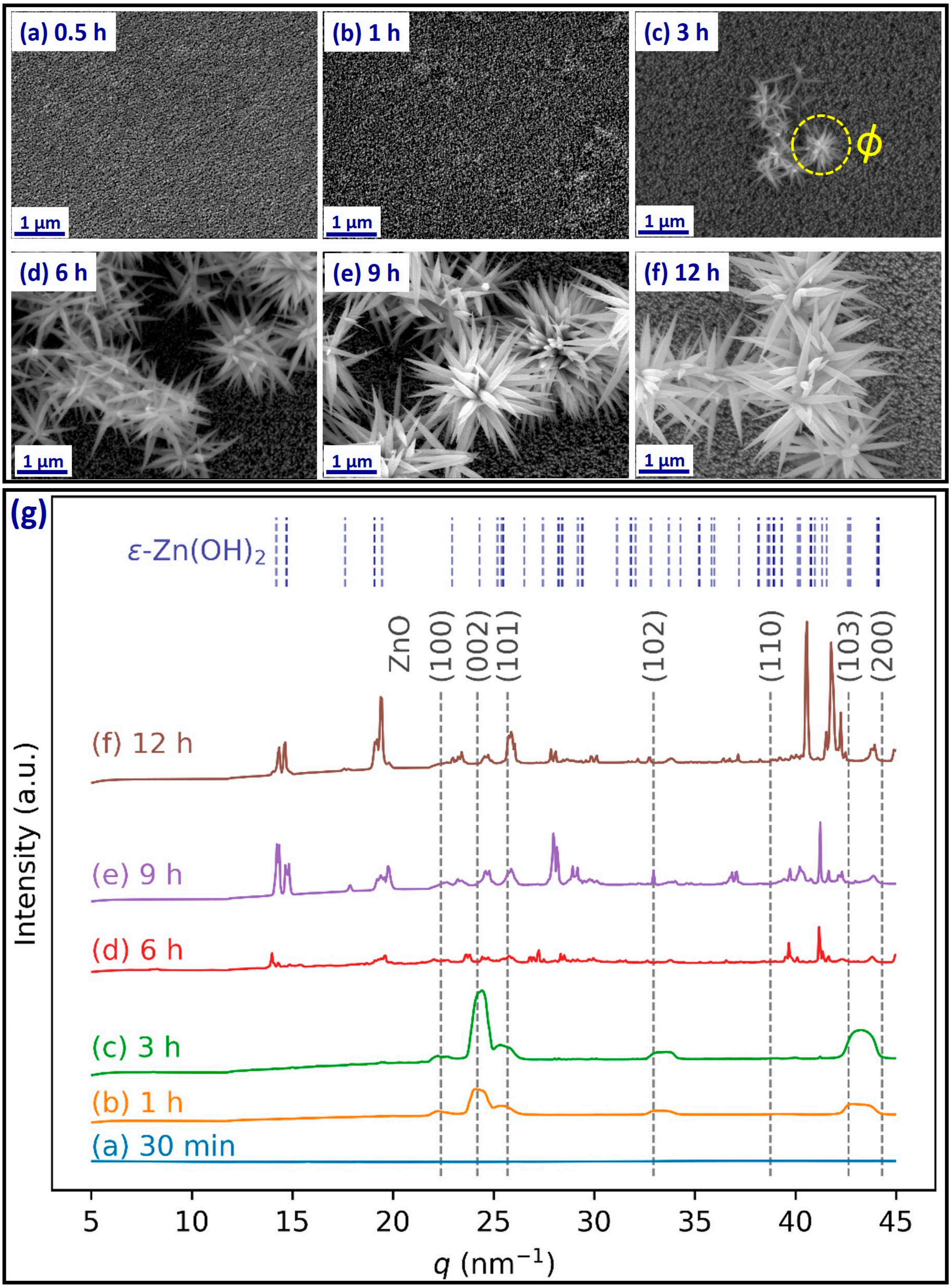

Figure 2: (a-f) SEM images of seeded silicon substrates in 5 mM zincate growth solution at different growth time intervals $t = 0.5 – 12$ h; and (g) corresponding GIXRD data for the substrates.

To evaluate the effect of substrate seeding on the ZnO urchin morphology, the one-step fabrication procedure was performed using unseeded silicon substrates (i.e. in 5 mM zincate solution at 20° C, and 12 h growth time). SEM image in Figure 3a shows that urchin like ZnO nanostructures were also obtained with a high surface coverage (Figure 3a, c), with urchins found on orthorhombic ε-Zn(OH)$_2$ crystal facets (Figure 3b). There was no significant difference in the urchin morphology (urchin size ϕ, needle length L, diameter D, and tip angle θ) compared to the seeded substrate. However, some urchins in the bare silicon area had a smaller number of nanoneedles (Figure 3d). Comparison of the XRD patterns in Figure S11 for the 12 h growth shows that, on the unseeded Si sample, the most intense peaks correspond to the ε-Zn(OH)$_2$ crystal structure, consistent with the SEM images shown in Figure 3.

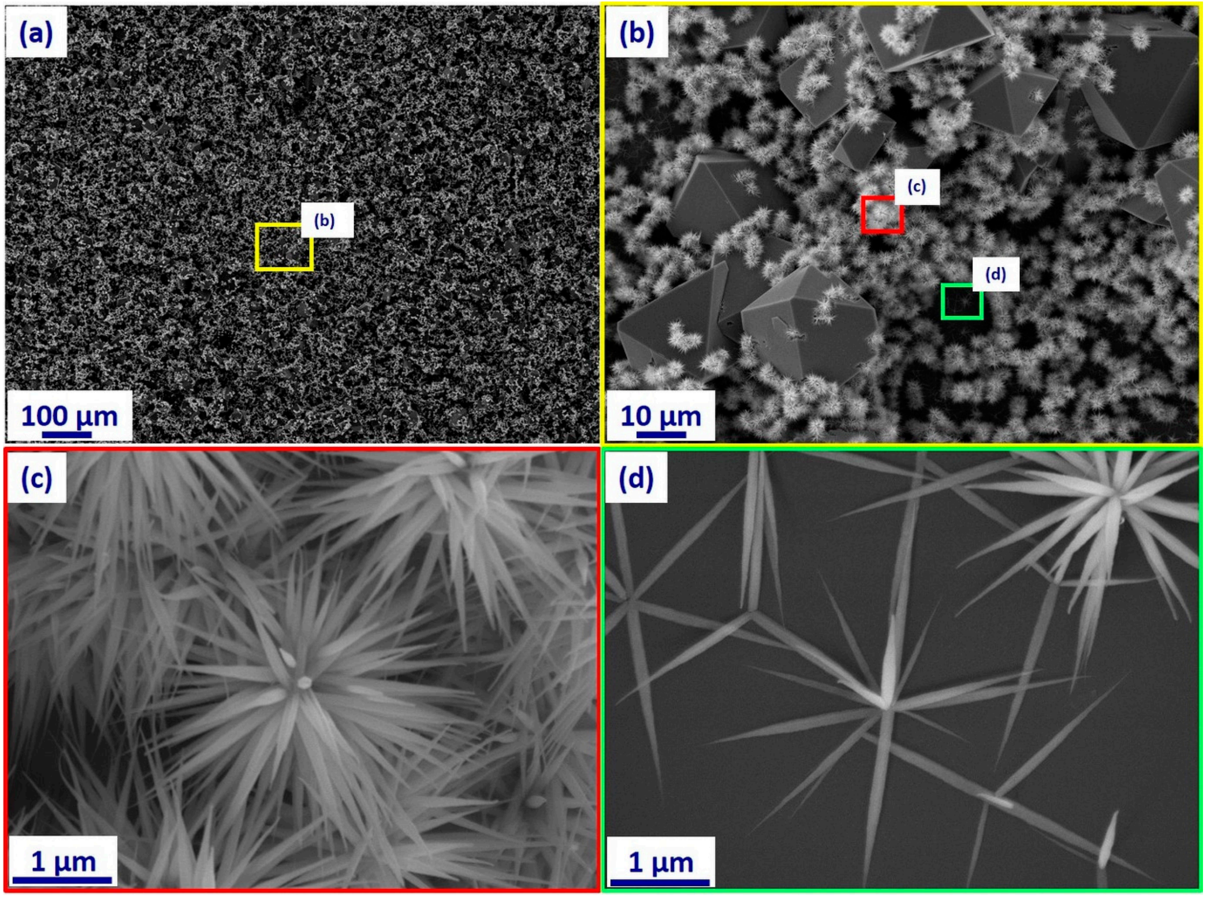

Figure 3: SEM images of ZnO nanostructures grown on the unseeded silicon substrate in the one-step synthesis (12 h, 20° C), with a high coverage of ZnO urchins (a) with morphology similar to that on seeded Si substrates (b, c). Orthorhombic ε-Zn(OH)$_2$ crystals were also observed (b) decorated with urchins. Urchins with a smaller number of needles were also observed in the bare silicon area (d).

Time dependant growth of ZnO urchins on non-seeded silicon substrate was also studied, and SEM images at different growth time intervals are shown in Figure S10. Similar to the seeded Si substrates, ZnO urchins emerged between 1-3 h of the growth time (Figure a, e), and their dimensions and surface coverage increased with time (Figure S10), with orthorhombic ε-Zn(OH)$_2$ crystals starting to appear on the surface between 3-6 h of the synthesis (Figure S10b).

Figure further compares the XRD on both seeded and non-seeded silicon substrates after the growth in the zincate solution for 12 h. Peaks corresponding to both ZnO (PDF 36-1451) and ε-Zn(OH)$_2$ (PDF 38-385) were identified, confirming their formation on the surfaces. The most intense peak in the seeded silicon sample corresponds to the ZnO (002) plane, which is the preferential growth direction of ZnO nanoneedles[57]. Along with the SEM images, this confirms that on seeded Si the primary growth led to ZnO nanoneedles, with the ZnO urchins grown atop in the secondary growth stage. In the case of the unseeded Si sample, the most intense peaks correspond to the ε-$Zn(OH)_2$ crystal structure. This is consistent with the SEM image (Figure 3b) which shows that the substrate was covered by ZnO urchins grown on orthorhombic $Zn(OH)_2$ crystals and bare Si surface, with a significantly smaller amount of arrayed ZnO nanoneedles (Figure d).

Growth of the ZnO nanoneedles and urchin structures were also trialled on copper sheets, soft PDMS and transparent glass substrates, all seeded by dipping the substrates in a solution of zinc acetate dihydrate in ethanol (Figure S1). The ZnO nanostructures grown on these surfaces (Figure g-i) exhibited similar urchin morphologies to the those on silicon substrates (Figure 1). The growth on glass was also evident, as it became translucent after the growth (Figure d and Figure S12). This demonstrates that the facile, room temperature synthesis method for ZnO nanoneedles and urchins is adaptable to various substrates.

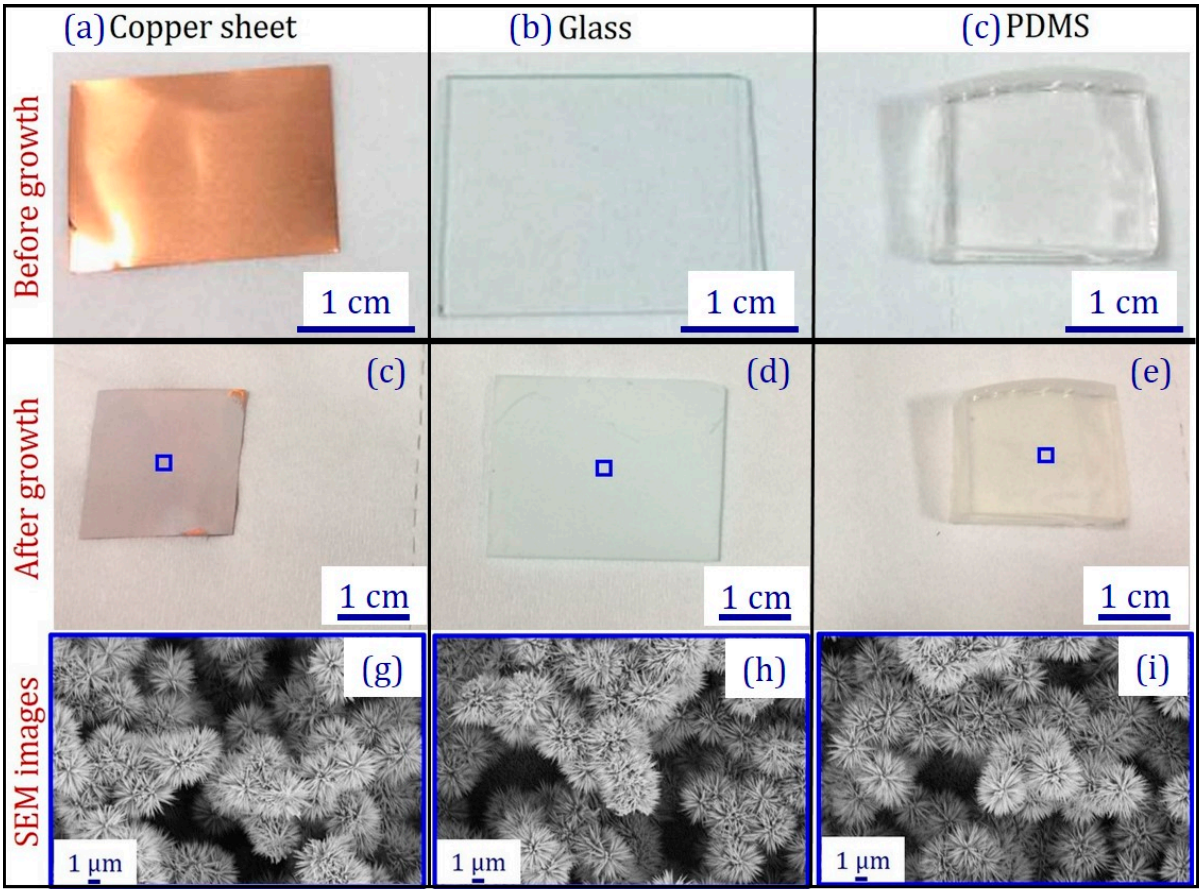

Figure 4: (a) Growth of ZnO urchin on seeded copper, glass slide and PDMS surfaces and the corresponding SEM images of the ZnO urchin formed on the substrates.

Si surfaces with ZnO urchins (both seeded and unseeded, 12 h growth time) were superhydrophilic, with a water droplet placed on these surfaces spreading completely and showing a water contact angle $\theta \sim 0^{\circ}$ (Table S1). They became superhydrophobic after overnight silanization (Table S1) with a static water contact angle $\theta \sim 159^{\circ} \pm 1.4^{\circ}$ (Figure 5a) and a contact angle hysteresis $\Delta\theta < 7^{\circ}$ was observed. For comparison, Table S1 shows that bare Si and Si coated with 20 nm ZnO thin film exhibited hydrophilic behaviour with a water static contact angle $\theta \sim 36^{\circ}$ and $\sim 61^{\circ}$, respectively.

To further demonstrate the superhydrophobicity in dynamic conditions, a 10 μL water droplet was allowed to fall on the silanized ZnO urchin surface from a height of 7 cm with a *Weber number* $We = \frac{\rho V^2 D_w}{\gamma} = 49$, where $\rho = 1$ g cm^{-3} is the density of water, $V = \sqrt{2gh}$=1.17 m s^{-1} the impact velocity of the falling droplet, γ = 73.8 mN m^{-1} the surface tension of water, and D_w = 2.67 mm the diameter of droplet (Table S1). The dynamic process was captured using a high-speed camera with a 10,000-fps capture rate. The water droplet bounced off the superhydrophic surface completely without leaving any visible residues, with a droplet-substrate contact time of 15.3 ms (Figure 5b and Video S1) which is close to the theoretical contact time $((\frac{\rho D_w^3}{\gamma})^{1/2} = 16.25$ ms) for water droplet on superhydrophobic surface[58].

In addition, the ZnO urchin coated surface also demonstrated anti-reflective behaviour. **Error! Reference source not found.**c shows <1% reflectance (R) over the wavelength range λ = 200-800 nm on the urchin surface, compared to two control samples (bare Si and Si with 20 nm ZnO thin film). There have been previous reports on fabrication of nanostructured anti-reflective surfaces [6,11,59–65]. Different techniques such as dry etching, wet etching, metal assisted etching, nanoimprint lithography, etching using O_2 plasma and inductively coupled plasma, optical lithography followed by etching etc.[66] have been used to fabricate such surfaces on silicon, polymers, and glass to achieve low reflectance. In comparison, the fabrication method we used to achieve the low reflectance (R < 1%) was simple with the synthesis undertaken at room temperature without the need for sophisticated instrumentation.

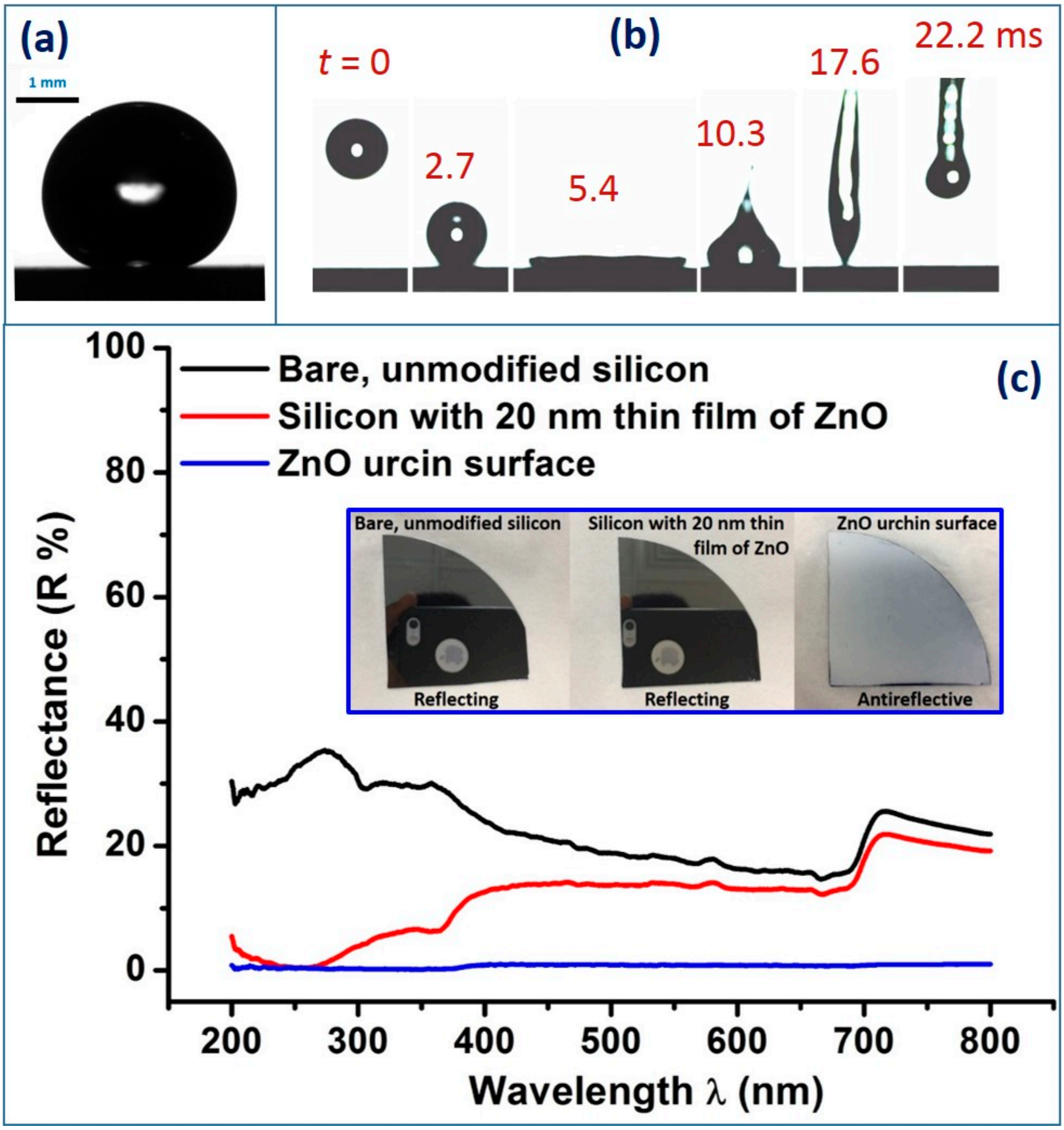

Figure 5: (a) Photograph of a 10 μL water droplet on ZnO urchin-coated surface after silanization, with a contact angle θ ~ 159°±1.4°. Prior to silanization, the surface was highly hydrophilic, displaying complete wetting by water with θ ~ 0° (Table S1). (b) High-speed camera images of a 10 μL droplet bouncing off the superhydrophobic ZnO urchin surface, with a contact time of 15.3 ms. (c) Reflectance from the ZnO urchin surface compared to the two control surfaces in the wavelength range λ= 200 – 800 nm. ZnO urchin surface was found to be the most anti-reflective with reflectance R < 1% over the whole wavelength range. The inset shows the highly reflective bare Si and Si with 20 nm ZnO film (with the reflection of the iPhone used to take the photo clearly visible), in contrast to the anti-reflective characteristic of the ZnO urchin surface.

To evaluate the bacterial interaction with the fabricated ZnO urchins on the seeded Si surface, it was submerged in 2 mL *E. coli* culture in phosphate-buffered saline (PBS) for 24 h and then imaged with SEM. This was compared with two control samples: unmodified bare Si and Si with a 20 nm sputtered ZnO film (Figure S13). SEM images in Error! Reference source not found.a (see also Table S2) show bacteria growth on the control surfaces; in contrast, no bacterium was observed on the ZnO nanostructured surface (Figure 6c, d). In addition, the SEM analysis revealed a change in the morphology of the ZnO urchins (inset in **Error! Reference source not found.**c): after 24 h immersion in the *E. coli* culture, the spiky urchin structure was transformed into the hexagonal pyramid structure (see Figure S14a). This can be attributed to the formation of sodium zinc phosphate hydrate ($NaZnPO_4.H_2O$)[67] due to the reaction between ZnO urchins and the PBS (*cf.* XRD data in Figure S14b). ZnO is known to exhibit antimicrobial efficacy[15–19], killing bacteria and prohibiting bacterial growth on its surface *via* release of Zn^{2+} ions which solicits generation of reactive oxygen species (ROS). A number of naturally occurring surfaces bearing spiky nanotextures (e.g. cicada wing, dragonfly wing, and gecko skin) have been reported to exhibit bactericidal efficacy, attributed to puncturing or stretching of the bacterial membrane, although the detailed mechanisms remain to be fully understood[3,11,68–71]. Hence, we suggest that the ZnO urchin surfaces could prevent bacterial growth by combining synergistically the inherent chemical activity of ZnO and the spiky morphology of the urchins that inhibits the bacteria to colonise on the surface of the ZnO urchins[18,72–74]. The sharp topography of the nanoneedles are particularly effective in disrupting the bacterial cell wall by imparting the localised stress on the bacterial membrane[75]. There are previous reports on reduced bacterial adhesion on superhydrophobic surfaces[76–79] where the antiwetting property of the surface plays a crucial role in the interaction of the bacteria with the surface; whereas our fabricated ZnO urchin surfaces exhibited bacteriophobic behaviour in a hydrophilic state (with a water contact angle $\theta \sim 0^{o}$).

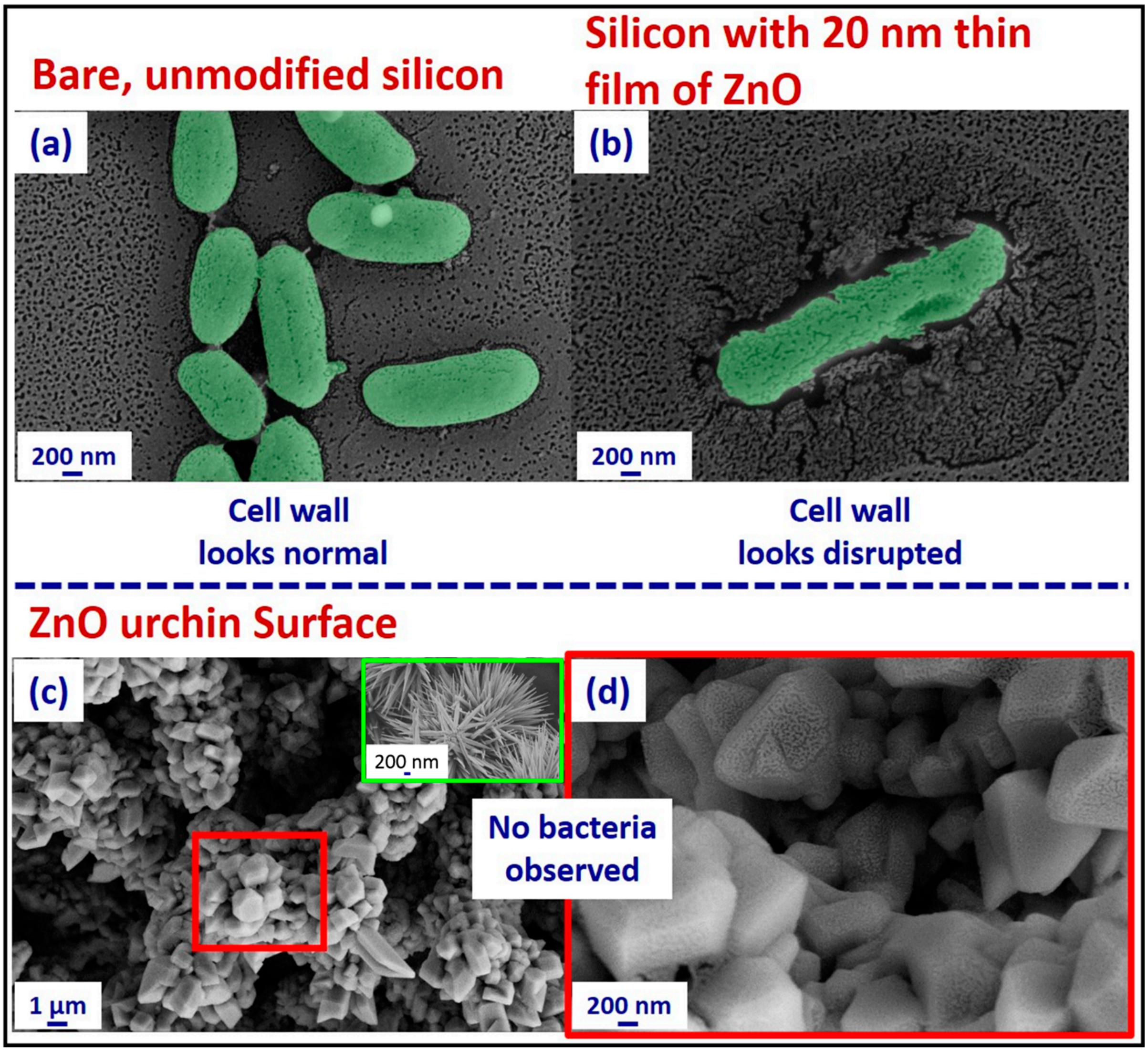

Figure 6: Representative SEM images of *E. coli* (false coloured Green) on different surfaces after 24 h of bacterial culture. (a) bare, unmodified silicon, (b) silicon with 20 nm thin film of ZnO and (c) & (d) ZnO urchin surface. Inset in Figure 6(c) shows the morphology of the ZnO urchin before bacterial culture on the urchin surface.

5. Conclusions

In summary, ZnO urchin structures were fabricated via a simple method involving submergence of a substrate (Si, PDMS, glass, or Cu) in an alkaline aqueous zincate ion ($Zn(OH)_4^{2-}$) solution at room temperature (~20° C). On the Si substrate seeded with ZnO nanocrystals, we observed ZnO urchin structures atop vertically aligned ZnO nanoneedles. The urchins consisted of densely packed, µm-long spiky ZnO nanoneedles radiating from the urchin centre, with a tapering angle of ~10°. The growth kinetics of the ZnO surface nanostructures was studied by time resolved SEM, revealing that the urchin morphology emerged at ~ 3 h reaction time with a small number of, but tapered, nanoneedles. The nanoneedle density and length then progressively increased with the reaction time. On the seeded Si substrate, a primary growth step of the vertical ZnO nanoneedles was identified preceding the secondary urchin growth. The ZnO urchin coated surface exhibited anti-reflective properties, reducing the reflectance to less than 1%. It was highly hydrophilic, with a water contact angle of ~0^o; after silanization, it exhibited superhydrophobicity with a water contact angle of 159° and hysteresis smaller than 7°. In addition, its dynamic hydrophobicity was demonstrated by bouncing-off of a water drop as captured by a high-speed camera, with resident time of 15.9 ms. Furthermore, the ZnO urchin surface showed bacteriophobic behaviour, as compared to the control Si and ZnO-coated surfaces, with no bacterium colonization observed on the surface after 24 h incubation in *E. coli*. The facile method for preparing ZnO urchins with unique morphology of tapered nanoneedles, and its ready adaptability to different surfaces (including polymers), may open new routes for fabrication of multifunctional ZnO nanostructured surfaces.

Supplementary Materials: The following are available online,

Figure S1: Process flow of the fabrication of ZnO nanostructures on seeded silicon substrates at near room temperature, **Figure S2:** SEM images of a silicon substrate seeded with ZnO nanoislands in 5 mM zinc acetate dihydrate solution (dipping × 5 times and annealed at 300° C for 30 minutes), **Figure S3:** Nanoneedle dimension measurement using ImageJ software. The values in the main text were averaged from 50 different needles, with the measurements of different parameters at each single needle repeated 5 times, **Figure S4:** Size distribution from ImageJ analysis of the nanoneedle tip diameter at the top D_t urchins ranging from 7-30 nm with an average diameter of $D_t = 13\pm7$ nm, **Figure S5:** Length of the nanoneedles L in the urchin structure vs. growth time. Length of the nanoneedle was found to increase with respect to synthesis time. Stars in figure shows that for time points 0, 0.5 and 1 h there was no formation of urchin structures, **Figure S6:** (a) the angled view after 9 h growth, showing ZnO urchins on the top of highly (b) oriented ZnO nanoneedles, **Figure S7:** Representative FESEM images of the seeded silicon substrate post 12 h synthesis in the zincate solution, **Figure S8:** SEM images of seeded silicon substrates after growth in zincate solution at different time intervals. Density of ZnO nano urchins was found to increase with the increase synthesis time, **Figure S9:** SEM images of seeded silicon substrates after growth in zincate solution at different time intervals. $Zn(OH)_2$ crystals were observed on the substrates for synthesis time $t > 3$ h, **Figure S10:** SEM images of ZnO urchins on a non-seeded silicon substrate, taken at different time intervals: (a) 3 h, (b) 6 h, (c) 9 h, and (d) 12 h. (e-h) show enlarged views of the square regions as labelled in (a-d), respectively, **Figure S11:** XRD of (a)&(b) seeded and (c)&(d) unseeded silicon substrates after growth in the zincate solution at 20° C for 12 h, with the ZnO and ε-$Zn(OH)_2$ peaks indicated by * and ▼, respectively, and the enlarged views shown on the right-hand side, **Figure S12:** Optical image showing the loss in transparency after the formation of ZnO urchin/nanoneedles on the glass substrate, **Figure S13:** 12 well culture plate for pouring the bacterial suspension on different samples, **Figure S14:** (a) SEM and (b) XRD of ZnO nanourchin surface after pouring the bacterial culture for 24 hours. Formation of sodium zinc phosphate hydrate ($NaZn\text{-}PO_4.H_2O$) was observed on the surface due to the reaction of ZnO with PBS leading to the change in morphology of the spiky ZnO nanowires, **Table S1:** Static contact angles of DI water droplet on different substrates, **Table S2:** SEM of *E. coli* on different substrates, **Video S1:** Superhydrophobic ZnO urchin.

Author Contributions: AT and WHB conceived and designed experiments; AT and PW designed, synthesised and characterised ZnO urchins; AT, SS, DN and PS performed experiments on anti-reflectivity, *E coli* colonisation, and dynamic superhydrophobicity of the urchin surfaces; PW, OB and WHB performed synchrotron XRD measurements. All authors contributed to data analysis and the manuscript writing.

Acknowledgments: AT acknowledges the funding from the British Council, United Kingdom and Department of Biotechnology, Government of India through the Newton-Bhabha PhD fellowship program. PW acknowledges the funding from the UK Engineering and Physical Sciences Research Council (EPSRC) through the Bristol Centre for Functional Nanomaterials (BCFN, grant no. EP/G036780/1). PS would like to thank the Ministry of Electronics and Information Technology, Government of India for the financial support. DPN acknowledges the funding by the Department of Biotechnology-Indian Institute of Science partnership program. W.H.B. would like to acknowledge funding from the EPSRC (EP/H034862/1 and Building Global Engagement in Research (BGER)), European Cooperation in Science and Technology (CMST COST) Action CM1101 "Colloidal Aspects of Nanoscience for Innovative Processes and Materials", and Marie Curie Initial Training Network (MCITN) on "Soft, Small, and Smart: Design, Assembly, and Dynamics of Novel Nanoparticles for Novel Industrial Applications" (NanoS3; FP7 Grant No. 290251). We acknowledge the beamline BM28 at the European Synchrotron Radiation Facility (a UK EPSRC funded facility) for beam time and the staff there for their help.

Conflicts of Interest: The authors declare no conflict of interest

References

(1) Tang, P.; Zhang, W.; Wang, Y.; Zhang, B.; Wang, H.; Lin, C.; Zhang, L. Effect of Superhydrophobic Surface of Titanium on Staphylococcus Aureus Adhesion. *J. Nanomater.* **2011**, *2011*, 1–8.

(2) Fadeeva, E.; Truong, V. K.; Stiesch, M.; Chichkov, B. N.; Crawford, R. J.; Wang, J.; Ivanova, E. P. Bacterial Retention on Superhydrophobic Titanium Surfaces Fabricated by Femtosecond Laser Ablation. *Langmuir* **2011**, *27* (6), 3012–3019.

(3) Ivanova, E. P.; Hasan, J.; Webb, H. K.; Truong, V. K.; Watson, G. S.; Watson, J. A.; Baulin, V. A.; Pogodin, S.; Wang, J. Y.; Tobin, M. J.; et al. Natural Bactericidal Surfaces: Mechanical Rupture of Pseudomonas Aeruginosa Cells by Cicada Wings. *Small* **2012**, *8* (16), 2489–2494.

(4) Pogodin, S.; Hasan, J.; Baulin, V. A.; Webb, H. K.; Truong, V. K.; Phong Nguyen, T. H.; Boshkovikj, V.; Fluke, C. J.; Watson, G. S.; Watson, J. A.; et al. Biophysical Model of Bacterial Cell Interactions with Nanopatterned Cicada Wing Surfaces. *Biophys. J.* **2013**, *104* (4), 835–840.

(5) Yao, C.; Webster, T. J.; Hedrick, M. Decreased Bacteria Density on Nanostructured Polyurethane. *J. Biomed. Mater. Res. - Part A* **2014**, *102* (6), 1823–1828.

(6) Chattopadhyay, S.; Huang, Y. F.; Jen, Y. J.; Ganguly, A.; Chen, K. H.; Chen, L. C. Anti-Reflecting and Photonic Nanostructures. *Mater. Sci. Eng. R Reports* **2010**, *69* (1–3), 1–35.

(7) Yamada, N.; Kim, O. N.; Tokimitsu, T.; Nakai, Y.; Masuda, H. Optimization of Anti-Reflection Moth-Eye Structures for Use in Crystalline Silicon Solar Cells. *Prog. Photovoltaics Res. Appl.* **2011**, *19* (2), 134–140.

(8) Park, H.; Shin, D.; Kang, G.; Baek, S.; Kim, K.; Padilla, W. J. Broadband Optical Antireflection Enhancement by Integrating Antireflective Nanoislands with Silicon Nanoconical-Frustum Arrays. *Adv. Mater.* **2011**, *23* (48), 5796–5800.

(9) Park, K.-C.; Choi, H. J.; Chang, C.-H.; Cohen, R. E.; McKinley, G. H.; Barbastathis, G. Nanotextured Silica Surfaces with Robust Superhydrophobicity and Omnidirectional Broadband Supertransmissivity. *ACS Nano* **2012**, *6* (5), 3789–3799.

(10) Zhang, D.; Yu, W.; Hao, D.; Li, L.; Liu, H.; Lu, Z. Functional Nanostructured Surfaces in Hybrid Sol–gel Glass in Large Area for Antireflective and Super-Hydrophobic Purposes. *J. Mater. Chem.* **2012**, *22* (33), 17328.

(11) Tripathy, A.; Sreedharan, S.; Bhaskarla, C.; Majumdar, S.; Peneti, S. K.; Nandi, D.; Sen, P. Enhancing the Bactericidal Efficacy of Nanostructured Multifunctional Surface Using an Ultrathin Metal Coating. *Langmuir* **2017**, *33* (44), 12569–12579.

(12) Zhang, Y.; Ram, M. K.; Stefanakos, E. K.; Goswami, D. Y. Synthesis, Characterization, and Applications

of ZnO Nanowires. *J. Nanomater.* **2012**, *2012*.

(13) Jones, F.; Tran, H.; Lindberg, D.; Zhao, L.; Hupa, M. Thermal Stability of Zinc Compounds. *Energy and Fuels* **2013**, *27* (10), 5663–5669.

(14) Makarona, E.; Athanassiou, B.; Prionistis, C.; Tegou, E.; Tsamis, C. A Cost-Efficient Solution-Based Process for the Development of ZnO Nanostructures: A Comprehensive Study of the Role of the Seeding Layer Formation Conditions. *Procedia Eng.* **2015**, *120*, 447–450.

(15) Kumar, R.; Umar, A.; Kumar, G.; Nalwa, H. S. Antimicrobial Properties of ZnO Nanomaterials: A Review. *Ceram. Int.* **2017**, *43* (5), 3940–3961.

(16) Xie, Y.; He, Y.; Irwin, P. L.; Jin, T.; Shi, X. Antibacterial Activity and Mechanism of Action of Zinc Oxide Nanoparticles against Campylobacter Jejuni. *Appl. Environ. Microbiol.* **2011**, *77* (7), 2325–2331.

(17) Sirelkhatim, A.; Mahmud, S.; Seeni, A.; Kaus, N. H. M.; Ann, L. C.; Bakhori, S. K. M.; Hasan, H.; Mohamad, D. Review on Zinc Oxide Nanoparticles: Antibacterial Activity and Toxicity Mechanism. *Nano-Micro Lett.* **2015**, *7* (3), 219–242.

(18) Tam, K. H.; Djurišić, A. B.; Chan, C. M. N.; Xi, Y. Y.; Tse, C. W.; Leung, Y. H.; Chan, W. K.; Leung, F. C. C.; Au, D. W. T. Antibacterial Activity of ZnO Nanorods Prepared by a Hydrothermal Method. *Thin Solid Films* **2008**, *516* (18), 6167–6174.

(19) Abinaya, C.; Mayandi, J.; Osborne, J.; Frost, M.; Ekstrum, C.; Pearce, J. M. Inhibition of Growth of S . Epidermidis by Hydrothermally Synthesized ZnO Nanoplates. *Mater. Res. Express.* **2017**, 4, 075401.

(20) Li, Z.; Yang, R.; Yu, M.; Bai, F.; Li, C.; Wang, Z. L.; Li, Z.; Yang, R.; Yu, M.; Bai, F.; et al. Cellular Level Biocompatibility and Biosafety of ZnO Nanowires. *J. Phys. Chem. C*, **2008**, *112* (November), 20114–20117.

(21) Li, P.; Liu, H.; Lu, B.; Wei, Y. Formation Mechanism of 1D ZnO Nanowhiskers in Aqueous Solution. *J. Phys. Chem. C* **2010**, *114* (49), 21132–21137.

(22) McBride, R. a.; Kelly, J. M.; McCormack, D. E. Growth of Well-Defined ZnO Microparticles by Hydroxide Ion Hydrolysis of Zinc Salts. *J. Mater. Chem.* **2003**, *13* (5), 1196–1201.

(23) Wang, J.; Hou, S.; Zhang, L.; Chen, J.; Xiang, L. Ultra-Rapid Formation of ZnO Hierarchical Structures from Dilution-Induced Supersaturated Solutions. *CrystEngComm* **2014**, *16* (30), 7115.

(24) You, T.; Yan, J.; Zhang, Z.; Li, J.; Tian, J.; Yun, J.; Zhao, W. Fabrication and Optical Properties of Needle-like ZnO Array by a Simple Hydrothermal Process. *Mater. Lett.* **2012**, *66* (1), 246–249.

(25) Safa, S. Enhanced UV-Detection Properties of Carbon Nanotube Impregnated ZnO Nanourchins. *Optik (Stuttg).* **2015**, *126* (19), 2194–2198.

(26) Ko, Y. H.; Yu, J. S. Tunable Growth of Urchin-Shaped ZnO Nanostructures on Patterned Transparent Substrates. *CrystEngComm* **2012**, *14* (18), 5824.

(27) Imani, R.; Drašler, B.; Kononenko, V.; Romih, T.; Eleršič, K.; Jelenc, J.; Junkar, I.; Remškar, M.; Drobne, D.; Kralj-Iglič, V.; et al. Growth of a Novel Nanostructured ZnO Urchin: Control of Cytotoxicity and Dissolution of the ZnO Urchin. *Nanoscale Res. Lett.* **2015**, *10* (1), 1–10.

(28) Banerjee, D.; Lao, J. Y.; Wang, D. Z.; Huang, J. Y.; Steeves, D.; Kimball, B.; Ren, Z. F. Synthesis and Photoluminescence Studies on ZnO Nanowires. *Nanotechnology* **2004**, *15* (3), 404–409.

(29) Wasik, P.; Redeker, C.; Dane, T. G.; Seddon, A. M.; Wu, H.; Briscoe, W. H. Hierarchical Surface Patterns upon Evaporation of a ZnO Nanofluid Droplet: Effect of Particle Morphology. *Langmuir* **2018**, *34* (4), 1645–1654.

(30) Wu, H.; Chen, L. X.; Zeng, X. Q.; Ren, T. H.; Briscoe, W. H. Self-Assembly in an Evaporating Nanofluid Droplet: Rapid Transformation of Nanorods into 3D Fibre Network Structures. *Soft Matter* **2014**, *10* (29), 5243–5248.

(31) Greene, L. E.; Law, M.; Tan, D. H.; Montano, M.; Goldberger, J.; Somorjai, G.; Yang, P. General Route to Vertical ZnO Nanowire Arrays Using Textured ZnO Seeds. *Nano Lett.* **2005**, *5* (7), 1231–1236.

(32) Wang, G.; Li, Z.; Li, M.; Feng, Y.; Li, W.; Lv, S.; Liao, J. Synthesizing Vertical Porous ZnO Nanowires Arrays on Si/ITO Substrate for Enhanced Photocatalysis. *Ceram. Int.* **2018**, *44* (2), 1291–1295.

(33) Gacusan, J.; Kobayashi, N. P.; Sanghadasa, M.; Meyyappan, M. Controlled Growth of Vertical ZnO Nanowires on Copper Substrate Controlled Growth of Vertical ZnO Nanowires on Copper Substrate. **2013**, *083105*.

(34) Wu, C.; Shen, L.; Yu, H.; Huang, Q.; Zhang, Y. C. Synthesis of Sn-Doped ZnO Nanorods and Their Photocatalytic Properties. *Mater. Res. Bull.* **2011**, *46* (7), 1107–1112.

(35) Solís-Pomar, F.; Martínez, E.; Meléndrez, M. F.; Pérez-Tijerina, E. Growth of Vertically Aligned ZnO Nanorods Using Textured ZnO Films. *Nanoscale Res. Lett.* **2011**, *6* (1), 524.

(36) Gurav, A. B.; Latthe, S. S.; Vhatkar, R. S.; Lee, J. G.; Kim, D. Y.; Park, J. J.; Yoon, S. S. Superhydrophobic Surface Decorated with Vertical ZnO Nanorods Modified by Stearic Acid. *Ceram. Int.* **2014**, *40* (5), 7151–7160.

(37) Lee, Y.; Zhang, Y.; Ng, S. L. G.; Kartawidjaja, F. C.; Wang, J. Hydrothermal Growth of Vertical ZnO Nanorods. *J. Am. Ceram. Soc.* **2009**, *92* (9), 1940–1945.

(38) Hu, J. Q.; Li, Q.; Meng, X. M.; Lee, C. S.; Lee, S. T. Thermal Reduction Route to the Fabrication of Coaxial Zn/ZnO Nanocables and ZnO Nanotubes. *Chem. Mater.* **2003**, *15* (1), 305–308.

(39) Riaz, M.; Fulati, A.; Amin, G.; Alvi, N. H.; Nur, O.; Willander, M. Buckling and Elastic Stability of Vertical ZnO Nanotubes and Nanorods. *J. Appl. Phys.* **2009**, *106* (3), 1–7.

(40) Sun, Y.; Riley, D. J.; Ashfbld, M. N. R. Mechanism of ZnO Nanotube Growth by Hydrothermal Methods on ZnO Film-Coated Si Substrates. *J. Phys. Chem. B* **2006**, *110* (31), 15186–15192.

(41) Katwal, G.; Paulose, M.; Rusakova, I. A.; Martinez, J. E.; Varghese, O. K. Rapid Growth of Zinc Oxide Nanotube-Nanowire Hybrid Architectures and Their Use in Breast Cancer-Related Volatile Organics Detection. *Nano Lett.* **2016**, *16* (5), 3014–3021.

(42) Wang, Y.; Cui, Z. Synthesis and Photoluminescence of Well Aligned ZnO Nanotube Arrays by a Simple Chemical Solution Method. *J. Phys. Conf. Ser.* **2009**, *152*, 012021.

(43) Wahab, R.; Ansari, S. G.; Kim, Y. S.; Seo, H. K.; Kim, G. S.; Khang, G.; Shin, H. S. Low Temperature Solution Synthesis and Characterization of ZnO Nano-Flowers. *Mater. Res. Bull.* **2007**, *42* (9), 1640–1648.

(44) Gokarna, A.; Parize, R.; Kadiri, H.; Nomenyo, K.; Patriarche, G.; Miska, P.; Lerondel, G. Highly Crystalline Urchin-like Structures Made of Ultra-Thin Zinc Oxide Nanowires. *RSC Adv.* **2014**, *4* (88), 47234–47239.

(45) Hieu, H. N.; Vuong, N. M.; Jung, H.; Jang, D. M.; Kim, D.; Kim, H.; Hong, S.-K. Optimization of a Zinc Oxide Urchin-like Structure for High-Performance Gas Sensing. *J. Mater. Chem.* **2012**, *22* (3), 1127–1134.

(46) Taheri, M.; Abdizadeh, H.; Golobostanfard, M. R. Formation of Urchin-like ZnO Nanostructures by Sol-Gel Electrophoretic Deposition for Photocatalytic Application. *J. Alloys Compd.* **2017**, *725*, 291–301.

(47) Shen, G.; Bando, Y.; Lee, C. J. Synthesis and Evolution of Novel Hollow ZnO Urchins by a Simple Thermal Evaporation Process. *J. Phys. Chem. B* **2005**, *109* (21), 10578–10583.

(48) Elias, J.; Bechelany, M.; Utke, I.; Erni, R.; Hosseini, D.; Michler, J.; Philippe, L. Urchin-Inspired Zinc Oxide as Building Blocks for Nanostructured Solar Cells. *Nano Energy* **2012**, *1* (5), 696–705.

(49) Newton, M. C.; Warburton, P. A. ZnO Tetrapod Nanocrystals. *Mater. Today* **2007**, *10* (5), 50–54.

(50) Modi, G. Zinc Oxide Tetrapod: A Morphology with Multifunctional Applications. *Adv. Nat. Sci. Nanosci. Nanotechnol.* **2015**, *6* (3).

(51) Neykova, N.; Brož, A.; Remeš, Z.; Hruška, K.; Kalbáčová, M.; Kromka, A.; Vaněček, M. ZnO Hedgehog-like Structures for Control Cell Cultivation. *Appl. Surf. Sci.* **2012**, *258* (8), 3485–3489.

(52) Bhaskarla, C.; Das, M.; Verma, T.; Kumar, A.; Mahadevan, S.; Nandi, D. Roles of Lon Protease and Its Substrate MarA during Sodium Salicylate-Mediated Growth Reduction and Antibiotic Resistance in Escherichia Coli. *Microbiol. (United Kingdom)* **2016**, *162* (5), 764–776.

(53) Sutton, S. Measurement of Microbial Cells by Optical Density. *J. Valid. Techn* **2011**, *17* (1), 46–49.

(54) Schneider, C. a; Rasband, W. S.; Eliceiri, K. W. NIH Image to ImageJ: 25 Years of Image Analysis. *Nat. Methods* **2012**, *9* (7), 671–675.

(55) Ashiotis, G.; Deschildre, A.; Nawaz, Z.; Wright, J. P.; Karkoulis, D.; Picca, F. E.; Kieffer, J. The Fast Azimuthal Integration Python Library: PyFAI. *J. Appl. Crystallogr.* **2015**, *48*, 510–519.

(56) Wu, X.; Bai, H.; Li, C.; Lu, G.; Shi, G. Controlled One-Step Fabrication of Highly Oriented ZnO Nanoneedle/Nanorods Arrays at near Room Temperature. *Chem. Commun. (Camb).* **2006**, No. 15, 1655–1657.

(57) Xu, S.; Wang, Z. L. One-Dimensional ZnO Nanostructures: Solution Growth and Functional Properties. *Nano Res.* **2011**, *4* (11), 1013–1098.

(58) CLANET, C.; BÉGUIN, C.; RICHARD, D.; QUÉRÉ, D. Maximal Deformation of an Impacting Drop. *J. Fluid Mech.* **2004**, *517*, 199–208.

(59) Han, Z. W.; Wang, Z.; Feng, X. M.; Li, B.; Mu, Z. Z.; Zhang, J. Q.; Niu, S. C.; Ren, L. Q. Antireflective Surface Inspired from Biology: A Review. *Biosurface and Biotribology* **2016**, *2* (4), 137–150.

(60) Diao, Z.; Dirks, J.-H.; Spatz, J. Bio-Inspired, Nanostructured Anti-Reflective Surfaces for Laser Applications. *Conf. Lasers Electro-Optics* **2016**, ATh3K.5.

(61) Boden, S. A.; Bagnall, D. M. Tunable Reflection Minima of Nanostructured Antireflective Surfaces. *Appl. Phys. Lett.* **2008**, *93* (13), 1–4.

(62) Zada, I.; Zhang, W.; Sun, P.; Imtiaz, M.; Abbas, W.; Zhang, D. Multifunctional , Angle Dependent Antireflection , and Hydrophilic Properties of SiO_2 Inspired by Nano-Scale Structures of Cicada Wings. *Appl. Phys. Lett.*, **2017**, 111, 153701.

(63) Chen, Y. C.; Huang, Z. S.; Yang, H. Cicada-Wing-Inspired Self-Cleaning Antireflection Coatings on Polymer Substrates. *ACS Appl. Mater. Interfaces* **2015**, *7* (45), 25495–25505.

(64) Morikawa, J.; Ryu, M.; Seniutinas, G.; Balčytis, A.; Maximova, K.; Wang, X.; Zamengo, M.; Ivanova, E. P.; Juodkazis, S. Nanostructured Antireflective and Thermoisolative Cicada Wings. *Langmuir* **2016**, *32* (18), 4698–4703.

(65) Tripathy, A.; Sen, P. Dragonfly Wing Inspired Multifunctional Antireflective Superhydrophobic Surfaces. In *2016 3rd International Conference on Emerging Electronics (ICEE)*; 2016; pp 1–3.

(66) Cai, J.; Qi, L. Recent Advances in Antireflective Surfaces Based on Nanostructure Arrays. *Mater. Horiz.* **2015**, *2* (1), 37–53.

(67) Liu, S.; Killen, E.; Lim, M.; Gunawan, C.; Amal, R. The Effect of Common Bacterial Growth Media on Zinc Oxide Thin Films: Identification of Reaction Products and Implications for the Toxicology of ZnO. *RSC Adv.* **2014**, *4* (9), 4363–4370.

(68) Tripathy, A.; Sen, P.; Su, B.; Briscoe, W. H. Natural and Bioinspired Nanostructured Bactericidal Surfaces. *Adv. Colloid Interface Sci.* **2017**, 248, 85-104.

(69) Ivanova, E. P.; Hasan, J.; Webb, H. K.; Gervinskas, G.; Juodkazis, S.; Truong, V. K.; Wu, A. H. F.; Lamb, R. N.; Baulin, V. A.; Watson, G. S.; et al. Bactericidal Activity of Black Silicon. *Nat. Commun.* **2013**, *4*, 1–7.

(70) Li, X.; Cheung, G. S.; Watson, G. S.; Watson, J. A.; Lin, S.; Schwarzkopf, L.; Green, D. W. The Nanotipped

Hairs of Gecko Skin and Biotemplated Replicas Impair and/or Kill Pathogenic Bacteria with High Efficiency. *Nanoscale* **2016**, *8* (45), 18860–18869.

(71) Tripathy, A.; Pahal, S.; Mudakavi, R. J.; Raichur, A. M.; Varma, M. M.; Sen, P. Impact of Bioinspired Nanotopography on the Antibacterial and Antibiofilm Efficacy of Chitosan. *Biomacromolecules* **2018**, 19, 4, 1340-1346.

(72) Zanni, E.; Bruni, E.; Chandraiahgari, C. R.; De Bellis, G.; Santangelo, M. G.; Leone, M.; Bregnocchi, A.; Mancini, P.; Sarto, M. S.; Uccelletti, D. Evaluation of the Antibacterial Power and Biocompatibility of Zinc Oxide Nanorods Decorated Graphene Nanoplatelets: New Perspectives for Antibiodeteriorative Approaches. *J. Nanobiotechnology* **2017**, *15* (1), 1–12.

(73) Okyay, T. O.; Bala, R. K.; Nguyen, H. N.; Atalay, R.; Bayam, Y.; Rodrigues, D. F. Antibacterial Properties and Mechanisms of Toxicity of Sonochemically Grown ZnO Nanorods. *RSC Adv.* **2015**, *5* (4), 2568–2575.

(74) Rago, I.; Chandraiahgari, C. R.; Bracciale, M. P.; De Bellis, G.; Zanni, E.; Cestelli Guidi, M.; Sali, D.; Broggi, A.; Palleschi, C.; Sarto, M. S.; et al. Zinc Oxide Microrods and Nanorods: Different Antibacterial Activity and Their Mode of Action against Gram-Positive Bacteria. *RSC Adv.* **2014**, *4* (99), 56031–56040.

(75) Li, X.; Chen, T. Enhancement and Suppression Effects of a Nanopatterned Surface on Bacterial Adhesion. *Phys. Rev. E* **2016**, *93* (5), 1–7.

(76) Zhang, X.; Wang, L.; Levänen, E. Superhydrophobic Surfaces for the Reduction of Bacterial Adhesion. *RSC Adv.* **2013**, *3* (30), 12003.

(77) Ma, J.; Sun, Y.; Gleichauf, K.; Lou, J.; Li, Q. Nanostructure on Taro Leaves Resists Fouling by Colloids and Bacteria under Submerged Conditions. *Langmuir* **2011**, *27* (16), 10035–10040.

(78) Truong, V. K.; Webb, H. K.; Fadeeva, E.; Chichkov, B. N.; Wu, A. H. F.; Lamb, R.; Wang, J. Y.; Crawford, R. J.; Ivanova, E. P. Air-Directed Attachment of Coccoid Bacteria to the Surface of Superhydrophobic Lotus-like Titanium. *Biofouling* **2012**, *28* (6), 539–550.

(79) Stallard, C. P.; McDonnell, K. A.; Onayemi, O. D.; O'Gara, J. P.; Dowling, D. P. Evaluation of Protein Adsorption on Atmospheric Plasma Deposited Coatings Exhibiting Superhydrophilic to Superhydrophobic Properties. *Biointerphases* **2012**, *7* (1–4), 1–12.

Table of Contents Graphic